Laminar Craya–Curtet jets

Antonio Revuelta[a)]
Departamento de Combustibles Fósiles, CIEMAT, 28040 Madrid, Spain

Carlos Martínez-Bazán and Antonio L. Sánchez
Area de Mecánica de Fluidos, Universidad Carlos III de Madrid, 28911 Leganés, Spain

Amable Liñán
E. T. S. I. Aeronáuticos, Plaza Cardenal Cisneros 3, Universidad Politécnica de Madrid, 28040 Madrid, Spain

(Received 24 June 2003; accepted 29 September 2003; published online 5 December 2003)

This Brief Communication investigates laminar Craya–Curtet flows, formed when a jet with moderately large Reynolds number discharges into a coaxial ducted flow of much larger radius. It is seen that the Craya–Curtet number, $C=(J_c/J_j)^{1/2}$, defined as the square root of the ratio of the momentum flux of the coflowing stream to that of the central jet, arises as the single governing parameter when the boundary-layer approximation is used to describe the resulting steady slender jet. The numerical integrations show that for C above a critical value C_c the resulting streamlines remain aligned with the axis, while for $C<C_c$ the entrainment demands of the jet cannot be satisfied by the coflow, and a toroidal recirculation region forms. The critical Craya–Curtet number is determined for both uniform and parabolic coflow, yielding $C_c=0.65$ and $C_c=0.77$, respectively. The streamlines determined numerically are compared with those obtained experimentally by flow visualizations, yielding good agreement in the resulting flow structure and also in the value of C_c. © *2004 American Institute of Physics.* [DOI: 10.1063/1.1629300]

Confined jet flows are of interest for many practical engineering applications. The configuration shown in Fig. 1, in which an axisymmetric jet of radius εa, with $\varepsilon \ll 1$, discharges into a coaxial ducted stream of radius a, is relevant in particular to ejector systems and combustion chambers. Most of the previous works have been devoted to the case of turbulent flows, corresponding to the high-Reynolds-number jets most often encountered in applications. Of particular relevance are the pioneering experimental and theoretical analyses of Craya and Curtet[1] and Curtet,[2] which addressed as a central issue the emergence of regions of reverse flow near the confining wall when sufficiently weak coflow is present. A dimensionless parameter based on similarity considerations was proposed to characterize the resulting flow, similar to that previously proposed by Thring and Newby in their study of turbulent, coflow diffusion flames,[3] for which the recirculating flow provides a key stabilizing mechanism. For the case of uniform coflow investigated by Craya and Curtet, their parameter reduces to $C=(J_c/J_j)^{1/2}$ in the limit $\varepsilon \to 0$ of small inner jet radius, where J_c and J_j represent the momentum fluxes of the coflow and of the jet, respectively. A detailed account of experimental results, theoretical analyses and approximate integral solutions for turbulent Craya–Curtet jets can be found in Ref. 4.

Unlike the above mentioned studies, we address here the laminar flow arising for values of the jet Reynolds number $R_j=[J_j/(\pi\rho)]^{1/2}/\nu \gg 1$ below a certain critical value, when the resulting symmetric solution remains steady, giving a slender jet of characteristic length $R_j\, a$ that can be described with relative errors of order R_j^{-2} with the boundary-layer (BL) approximation. The same incompressible fluid of density ρ and kinematic viscosity ν is assumed to be present in both streams. In the analysis, the ratio of the inner to the outer radii ε will be assumed to be very small, as done in Ref. 5 for the confined jet with no coflow, and the momentum flux of the coflow J_c will be assumed to be comparable to that of the jet, i.e., Craya–Curtet numbers $C=(J_c/J_j)^{1/2}$ of order unity, the latter being the appropriate distinguished limit for studying the emergence of reverse flow. Although much research has been done on confined laminar jets (see, e.g., the literature review given in Ref. 5), the study of coflow laminar jets in this limit has not been attempted in the past. As shown below, the use of the BL approximation provides a simple way to evaluate, for the moderately large values of R_j typical of many small-scale flow devices, the critical conditions for existence of recirculating flow, a result that is independent of R_j. The resulting flow structure depends on the shape of the initial coflow velocity profile, but is independent of the downstream boundary conditions, provided the confining duct is longer than the resulting recirculating region. The BL analysis also gives the dependence of the flow scales, e.g., length of recirculating region, on R_j.

The characteristic lengths $R_j a$ and a will be used as scales to define the dimensionless axial and radial coordinates, x and r, while the characteristic velocities $u_0=[J_j/(\pi\rho)]^{1/2}/a$ and ν/a will be used as scales for the dimensionless axial and radial velocities u and v and the characteristic dynamic pressure ρu_0^2 will be employed to scale

a)Electronic mail: a.revuelta@ciemat.es

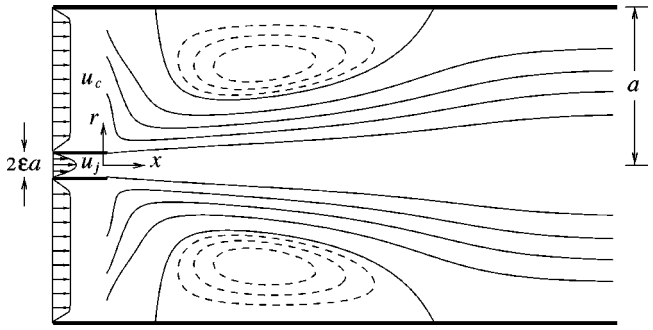

FIG. 1. The Craya–Curtet configuration studied here with the streamlines obtained from integration of (1)–(4) for $\varepsilon=0.07$ and $C=0.3$.

the pressure differences from the entrance value p. Use of these dimensionless variables reduces the BL equations to

$$\frac{\partial u}{\partial x}+\frac{1}{r}\frac{\partial(rv)}{\partial r}=0, \tag{1}$$

$$u\frac{\partial u}{\partial x}+v\frac{\partial u}{\partial r}=-\frac{dp}{dx}+\frac{1}{r}\frac{\partial}{\partial r}\left(r\frac{\partial u}{\partial r}\right), \tag{2}$$

to be integrated with boundary conditions

$$\partial u/\partial r=v=0 \quad \text{at} \quad r=0$$

and

$$u=v=0 \quad \text{at} \quad r=1 \tag{3}$$

and with initial condition at $x=0$

$$u=u_j(r) \quad \text{for} \quad 0<r<\varepsilon$$

and

$$u=u_c(r) \quad \text{for} \quad \varepsilon<r<1. \tag{4}$$

Note that, with the scales used, the initial momentum fluxes of the jet and of the coflow must satisfy $\int_0^\varepsilon 2ru_j^2dr=1$ and $\int_\varepsilon^1 2ru_c^2dr=C^2=J_c/J_j$. Problems (1)–(4) can be integrated for given values of ε and C and for different shapes of the initial velocity distributions. In particular, the streamlines shown in Fig. 1 correspond to $\varepsilon=0.07$ and $C=0.3$ with uniform velocity profiles $u_j=\varepsilon^{-1}$ and $u_c/C=(1-\varepsilon^2)^{-1/2}$, a case for which a robust toroidal vortex is formed. As in the rest of the integrations presented below, a pseudotransient finite-volume scheme was used to integrate the BL equations.

The problem simplifies further when, as typically occurs in many applications, the value of ε is small. To provide a coflow momentum flux $J_c\sim J_j$, the velocity at the jet exit u_j must be a factor ε^{-1} larger than $u_c\sim u_0$. Despite this large velocity, the associated jet volume flux becomes a factor ε smaller than that of the coflow, so that the jet behaves in the first approximation as a point source of momentum with negligible volume flux. Initially, the jet develops over a distance of order $x\sim\varepsilon\ll 1$ as a free jet discharging into a stagnant atmosphere, approaching for distances x in the range $\varepsilon\ll x\ll 1$ the self-similar Schlichting solution[6] $u=3/(8x)[1+(3/64)(r/x)^2]^{-2}$ independent of the shape of the initial velocity profile u_j. This solution must be supplemented with the solution emerging in the coflow stream at small distances $\varepsilon\ll x\ll 1$, which will be obtained below for two limiting cases of practical interest: the initial uniform profile $u_c=C$ and the fully developed profile $u_c=\sqrt{3}C(1-r^2)$.

With uniform coflow, the solution in the outer stream at distances $\varepsilon\ll x\ll 1$ posseses a uniform-velocity core where $u=C(1+K_1x^{1/2}+K_2x+\cdots)$ and $dp/dx=-C^2[(K_1/2)x^{-1/2}+(K_1^2/2+K_2)+\cdots]$, with $K_1,K_2,\cdots$ being constants that depend on the combined effect of the constant entrainment rate $rv=-4$ at the axis associated with Schlichting solution and of the boundary layer of characteristic thickness $x^{1/2}$ that develops on the outer wall, with the latter being the dominant effect. As in the case of the entry flow in a circular pipe[7] discussed by Atkinson and Goldstein in Ref. 8, the solution for the boundary layer requires the introduction of an expansion $\psi=-C[(C/x)^{1/2}f_1(\eta)+C/x\ f_2(\eta)+\ldots]$ for the stream function, where $\eta=(C/x)^{1/2}(1-r^2)/4$ is the appropriate local coordinate. The solution for f_1, which corresponds to the Blasius boundary layer over a flat plate,[9] determines the value of $K_1=3.4415$ when overall constant volume flux is imposed.[7] The constant $K_2=-17.0961$, on the other hand, needs to account for the following correction f_2 in the wall boundary layer, and also for the fluid volume $-8\pi x$ entrained by the jet. Combining the uniform core, the boundary layer and the jet yields

$$u=\frac{3}{8x}\left[1+\frac{3}{64}\left(\frac{r}{x}\right)^2\right]^{-2}+\frac{C}{2}\left[\dot{f}_1+\left(\frac{C}{x}\right)^{1/2}\dot{f}_2+\ldots\right] \tag{5}$$

as a composite expansion for the velocity distribution, where the dot $\dot{}$ denotes differentiation with respect to η.

The solution is different for developed coflow $u_c=\sqrt{3}C(1-r^2)$, when changes in the outer stream are driven by the jet entrainment, leading for $\varepsilon\ll x\ll 1$ to a solution of the form $u=\sqrt{3}C(1-r^2)-8x+\cdots$, $rv=-4(1-r^2)+\cdots$, and $dp/dx=-4\sqrt{3}C+(\sqrt{3}C/2)^{1/3}Px^{1/3}+\cdot$, where the constant P is determined by matching this outer solution with the boundary layer, of characteristic thickness $x^{-1/3}$, that develops on the wall. Within this boundady layer, the velocity can be expressed as $u=4(\sqrt{3}C/2)^{2/3}\xi x^{1/3}-2(\sqrt{3}C/2)^{1/3}\xi^2x^{2/3}+f'x+\cdots$ and $rv=(\sqrt{3}C/2)^{-1/3}(4f/3-\xi f'/3)x^{1/3}+\cdots$ in terms of the rescaled stream function $f(\xi)$, with the prime $'$ denoting differentiation with respect to the boundary-layer coordinate $\xi=(\sqrt{3}C/2)^{1/3}(1-r)/x^{1/3}$. The solution reduces to that of integrating $f'''+4\xi^2f''/3-16\xi f'/3+16f/3=P$ with boundary conditions $f(0)=f'(0)=f'(\infty)+8=0$, a problem that determines in particular the value of $P=17.528$. At the order calculated here, the composite expansion

$$u=\frac{3}{8x}\left[1+\frac{3}{64}\left(\frac{r}{x}\right)^2\right]^{-2}+\sqrt{3}C(1-r^2)+f'x, \tag{6}$$

represents uniformly the velocity distribution for $\varepsilon\ll x\ll 1$.

Hence, the limit of large jet Reynolds numbers $R_j\gg 1$ and large expansion ratios $\varepsilon\ll 1$ reduces the problem in the first approximation to that of integrating (1) and (2) with boundary conditions (3) and with the initial conditions given in (4) replaced in the integrations with the profiles (5) (uniform coflow) or (6) (fully developed coflow) evaluated at $x\ll 1$. As anticipated above, the Craya–Curtet number C emerges as the single governing parameter, which was varied

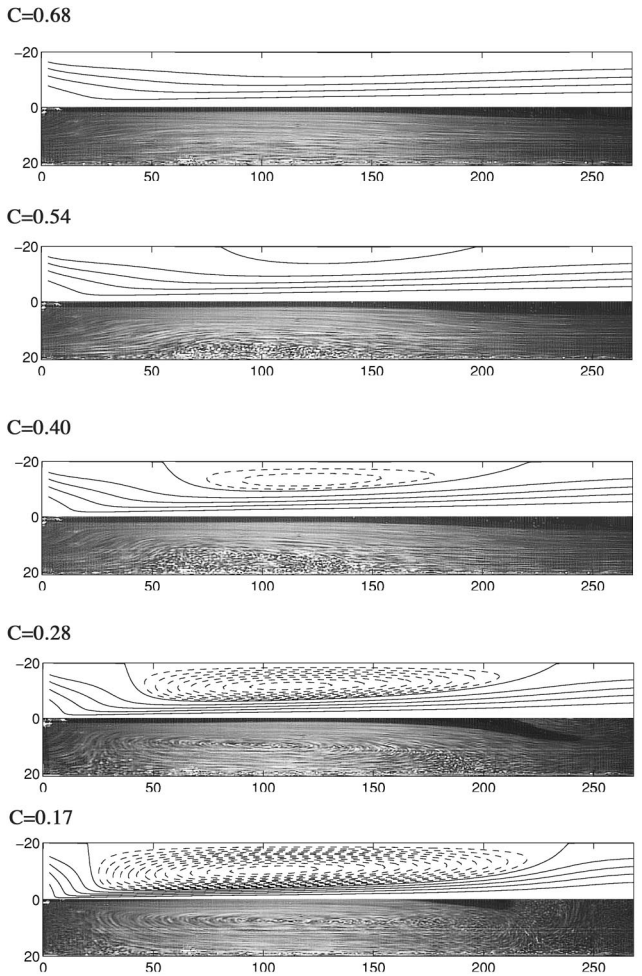

FIG. 2. Streamlines obtained by numerical integration of the boundary-layer equations for $\varepsilon=0$ (upper half of each plot) and by laser induced fluorescence (lower half of each plot).

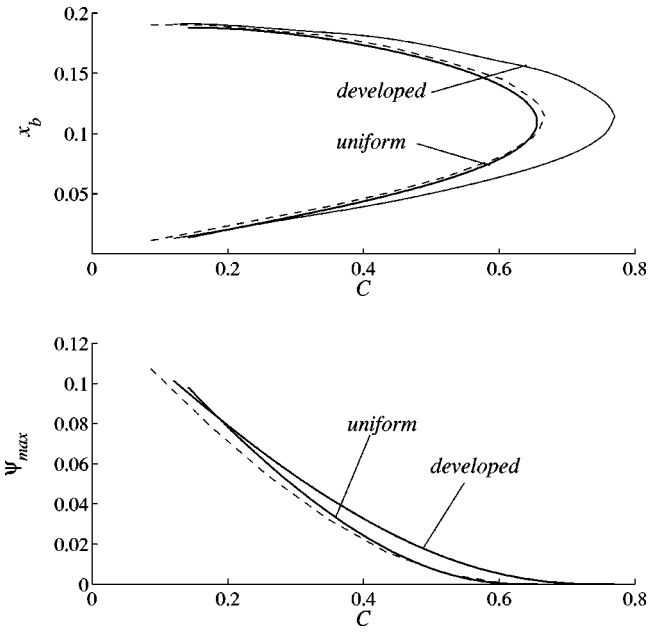

FIG. 3. The variation with C of the upstream and downstream ends of the recirculation region and of the maximum value of the stream function with uniform and parabolic coflow; the dashed lines are the results with parabolic coflow represented in terms of C^*.

in the integrations, giving the results of Figs. 2–4. Figure 2 shows the streamlines determined numerically with uniform coflow for five different Craya–Curtet numbers. The toroidal eddy arising for $C<C_c$, with $C_c=0.65$ for uniform coflow and $C_c=0.77$ for fully developed coflow, is clearly observed in the plots. To enable comparisons with the experimental results discussed below, the radial and axial coordinates are displayed in their dimensional form $a\,r$ and $R_j\,a\,x$, with the values of $R_j=35$ and $a=20$ mm corresponding to the experimental conditions.

To characterize the recirculating flow, the locations at which the dividing streamline intersects the wall are given as a function of C in Fig. 3, which also shows the maximum value of the stream function ψ within the vortex, with ψ defined in the usual manner and $\psi=0$ on the wall. As can be seen, the length of the vortex and the volume flux of recirculating fluid, measured by $\psi_{\max}$, decrease as C_c is approached. The curves indicate in particular that for $C\gtrsim 0.6$ the fluid trapped in the recirculating eddy, still of nonnegligible size, is nearly stagnant.

Figure 4 shows the distribution of pressure downstream from the jet exit as obtained for parabolic coflow. As can be seen, the pressure gradient increases from the initial value $dp/dx=-4\sqrt{3}C$ to reach a maximum near the center of the recirculating region, and then decreases to recover the same value $dp/dx=-4\sqrt{3}C$ sufficiently far downstream. As a result, the pressure increases from the entrance value to reach a maximum and then decreases linearly in the final Poiseuille region. The results are similar with uniform coflow, with differences being more noticeable near the entrance, where $dp/dx\propto x^{-1/2}$. Note that the type of results given in Fig. 4 are of interest when the jet is used as an ejector system, with

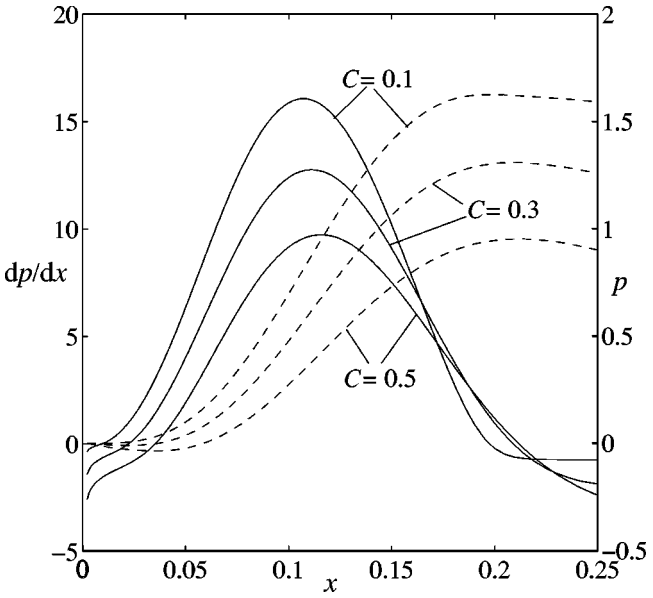

FIG. 4. The variation with x of the pressure gradient (solid lines) and of the pressure difference from the entrance value (dashed lines) for different C as obtained from numerical integrations with initial parabolic coflow.

the curves $p(x)$ relating the pressure jump, the duct length, and the momentum flux of the inner jet with the resulting coflow.

As seen in the comparison of Fig. 3, the flow structure depends on the velocity distribution in the coflow. When parabolic coflow is considered, the existence of relatively small velocities in the vicinity of $r=1$ clearly facilitates the appearance of reverse flow for a larger C_c. Use of an alternative governing parameter, C^*, incorporating the influence of the nonuniform coflow momentum distribution, may reduce this dependence. Among the different possibilities, one may for instance use the coflow volume flux Q_c to define $C^*=[Q_c/(\sqrt{\pi}a)]/(J_j/\rho)^{1/2}$ as the ratio of the characteristic coflow velocity $Q_c/(\pi a^2)$ to the characteristic velocity $u_0=(J_j/\rho\pi)^{1/2}/a$. This alternative definition yields $C^*=C$ for uniform coflow and $C^*=\sqrt{3}C/2$ for parabolic coflow, so that in terms of C^* criticality is achieved at $C_c^*\simeq 0.65$ for uniform coflow and at $C_c^*\simeq 0.67$ for parabolic coflow. Also remarkable is the agreement observed in Fig. 3 when the results of the parabolic coflow are represented in terms of C^*.

To validate the BL results given above, experiments were performed for moderately large values of R_j and ε^{-1}. A water jet was injected through a hypodermic vertical needle of inner radius equal to $\varepsilon a=0.597$ mm into a coaxial water stream confined by a cylindrical glass duct of radius $a=20$ mm ($\varepsilon\approx 0.03$). The flow rates were accurately controlled by separate flowmeters provided with high-precision valves. Constant-head water supplies were employed to avoid pressure fluctuations in the feeding lines. To visualize the streamlines, the coflow stream was seeded with neutrally buoyant particles of mean diameter equal to 5 μm. A 2 W argon–ion laser source was employed to produce a laser sheet using a cylindrical lens. The light scattered by the particles was captured with a charge coupled device camera and digitally enhanced afterwards, producing the images shown in Fig. 2. Streamlines are clearly visible in regions of sufficiently large velocity, whereas in the vicinity of the wall and also within the toroidal vortex for $0<C_c-C\ll 1$, where the flow is nearly stagnant, the existence of still standing particles results in a grainy region. For the experimental results reported here, the Reynolds number of the jet was maintained at the constant value $R_j=35$, while the coflow was reduced to obtain decreasing values of C. Recirculation was first observed for $C_c=0.68$, a value slightly above that predicted by the BL calculation. For smaller values of C both the length and the width of the recirculating region are seen to increase, in agreement with the numerical results. The discrepancy in C_c results in larger differences in flow structure in comparisons for $C=0.68$ and $C=0.54$, with no reverse flow appearing in the numerical results for $C=0.68$ and with the recirculating region determined experimentally for $C=0.54$ being larger and located upstream from that determined numerically. Much better agreement is observed in the plots for $C=0.40$, $C=0.28$, and $C=0.17$. It can be expected that the accuracy of the BL approximation would improve for larger R_j, a point supported by comparisons with integrations of the complete Navier–Stokes equations computed in Ref. 5 for confined jets with no coflow. Nevertheless, considering the moderate values of the parameters $R_j=35$ and $\varepsilon^{-1}\simeq 34.8$ used in the experiment, the comparisons of Fig. 2 are sufficiently satisfactory, and demonstrate the applicability of the BL approximation combined with the limit $\varepsilon=0$ to describe laminar Craya–Curtet jets with finite Reynolds number and finite expansion ratios.

It is worth mentioning that the boundary-layer computation given above also applies to turbulent Craya–Curtet jets, when use is made of a constant turbulent viscosity ν_T to model turbulent stresses. The value $C_c=0.65$ determined with this simple Boussinesq approach agrees reasonably well with the value $C_c\simeq 0.75$ obtained experimentally[10] for turbulent confined jets with uniform coflow and $\varepsilon\ll 1$. In using this approximation, it seems appropriate to select for the constant turbulent viscosity the value $\nu_T=0.0316[J_j/(\pi\rho)]^{1/2}$ for which the associated Schlichting solution matches the spreading angle measured experimentally for a free turbulent jet.[11] Note that the apparent Reynolds number based on the turbulent viscosity becomes $R_j=[J_j/(\pi\rho)]^{1/2}/\nu_T=31.62$, so that in this approximation the streamlines given in Fig. 2 for $R_j=35$ represent approximately the mean motion of turbulent Craya–Curtet jets.

ACKNOWLEDGMENTS

This collaborative research was supported by the Spanish MCyT under Project No. DPI2002-04550-C07. Fruitful discussions with Dr. Marcos Vera are gratefully acknowledged.

[1] A. Craya and R. Curtet, "Sur l'evolution d'un jet en espace confine," C. R. Acad. Sci., Paris **241**, 621 (1955).
[2] R. Curtet, "Confined jets and recirculation phenomena with cold air," Combust. Flame **2**, 383 (1958).
[3] M. W. Thring and M. P. Newby, "Combustion length of enclosed turbulent jet flames," Proc. Combust. Institute **4**, 789 (1953).
[4] N. Rajaratnam, *Turbulent Jets* (Elsevier, Amsterdam, 1976), pp. 148–183.
[5] A. Revuelta, A. L. Sánchez, and A. Liñán, "Confined axisymmetric laminar jets with large expansion ratios," J. Fluid Mech. **456**, 319 (2002).
[6] H. Schlichting, "Laminare strahlausbreitung," Z. Angew. Math. Mech. **13**, 260 (1933).
[7] L. Rosenhead, *Laminar Boundary Layers* (Dover, New York, 1963), pp. 439–446.
[8] S. Goldstein, *Modern Developments in Fluid Mechanics* (Clarendon, Oxford, 1938).
[9] H. Blasius, "Grenzschichten in Flüssigkeiten mit kleiner Reibung," Z. Math. Phys. **56**, 1 (1908).
[10] H. A. Becker, H. C. Hottel, and G. C. Williams, "Mixing and flow in ducted turbulent jets," Proc. Combust. Institute **9**, 7 (1962).
[11] H. J. Hussein, S. C. Capp, and W. K. George, "Velocity measurements in a high-Reynolds-number, momentum-conserving, axisymmetric, turbulent jet," J. Fluid Mech. **258**, 31 (1994).